K^- particles are considered in conjunction with the results of GVW, the depth of the effective nucleus–Σ scattering potential and the size of the cross section in nuclei for $\Sigma^\pm$ absorption (by conversion to a Λ^0 or Σ^0) are related by the model presented here. If the effective nuclear potential well for low-energy sigmas is attractive and shallow ($V_\Sigma \approx -10$ Mev), the $\Sigma^\pm$ absorption cross section in nuclei must be reasonably strong, $\sigma_a \approx 10$ millibarns. On the other hand, if the well is attractive and deep ($V_\Sigma < -25$ Mev), the absorption must be weak ($\sigma_a \lesssim 5$ millibarns). It is believed that an attractive Σ potential deeper than 35 Mev would inhibit the emission of $\Sigma^\pm$ sufficiently to be in contradiction with the experimental results, even if the absorption cross section σ_a were quite small.

These rough estimates concerning the charged–Σ absorption could be made with much improved accuracy if more were known about the relative strengths of K^- absorption by neutrons and protons. It is hoped that more information concerning the K^-–n absorption will be obtained soon by experiments in deuterium bubble chambers. Eventually, of course, direct measurements of Σ–particle absorption and scattering by nuclei and nucleons will be made.

ACKNOWLEDGMENTS

The author wishes to thank Dr. R. Stephen White, Dr. Francis C. Gilbert, Dr. Warren Heckrotte, Professor Gerson Goldhaber, and Dr. Sulamith Goldhaber for helpful discussions concerning this problem.

PHYSICAL REVIEW VOLUME 107, NUMBER 1 JULY 1, 1957

Cross Sections for Antiprotons in Hydrogen, Beryllium, Carbon, and Lead*

BRUCE CORK, GLEN R. LAMBERTSON, ORESTE PICCIONI,† AND WILLIAM A. WENZEL
Radiation Laboratory, University of California, Berkeley, California

(Received February 18, 1957)

A strong-focusing momentum channel has been arranged to form a beam from antiprotons produced by 6.0-Bev protons striking an internal target of the Bevatron. The channel consists of five 4-inch-diameter magnetic quadrupole lenses and two deflecting magnets adjusted to give a $\pm 5\%$ momentum interval. The antiprotons were selected from a large background of mesons by a scintillation counter telescope with a time-of-flight coincidence circuit having a resolution of $\pm 2 \times 10^{-9}$ second. This system allowed detection of approximately 400 antiprotons per hour. With a liquid hydrogen attenuator, the total antiproton-proton cross section at four different energies, 190, 300, 500, and 700 Mev, has been observed to be 135, 104, 97, and 94 mb, respectively. Also, the total cross sections for antiprotons incident on Be and C have been measured at two energies. The inelastic cross sections for carbon have been measured by observing the pulse heights produced by the interactions in a target of liquid scintillator. To measure the inelastic cross section for a high-Z element, lead wafers were immersed in the liquid scintillator, and to select inelastic events the pulse heights were measured.

I. INTRODUCTION

PREVIOUS experiments have shown that the antiproton interacts strongly with matter.[1–4] At 500 Mev for lead glass, copper, and beryllium, and at lower energies for photographic emulsions, the absorption cross section is significantly greater than geometric. The purpose of the experiment reported here was to extend to other elements the measurements on the interaction of antiprotons and, in particular, to measure as a function of energy the total proton-antiproton cross section, which is of central importance to the understanding of the nucleon-antinucleon interaction.

In order to fit the experimental program into a feasible time schedule, considerable effort was spent in the development of a usable antiproton beam of high intensity. The use of this beam in the production and identification of antineutrons has been described in an earlier report.[5]

The magnetic channel and the basic electronics are described in Secs. II and III, respectively, while operation of the antiproton identification scheme is included in Sec. IV. The attenuation experiment in hydrogen is described in Sec. V; and the measurements on beryllium, carbon, and lead in Sec. VI.

II. MAGNETIC BEAM CHANNEL

Antiprotons were produced in a 6-inch-long beryllium target in the internal beam of the Bevatron (Fig. 1).

* This work was done under the auspices of the U. S. Atomic Energy Commission.

† On leave from Brookhaven National Laboratory, Upton, New York.

[1] Brabant, Cork, Horwitz, Moyer, Murray, Wallace, and Wenzel, Phys. Rev. **101**, 498 (1956), and **102**, 1622–1626 (1956).

[2] Chamberlain, Keller, Segrè, Steiner, Wiegand, and Ypsilantis, Phys. Rev. **102**, 1637 (1956).

[3] Chamberlain, Chupp, Ekspong, Goldhaber, Goldhaber, Lofgren, Segrè, Wiegand, Amaldi, Baroni, Castagnoli, Franzinetti, and Manfredini, Phys. Rev. **102**, 921 (1956).

[4] Barkas, Birge, Chupp, Ekspong, Goldhaber, Goldhaber, Heckman, Perkins, Sandweiss, Segrè, Smith, Stork, Van Rossum, Amaldi, Baroni, Castagnoli, Franzinetti, and Manfredini, Phys. Rev. **105**, 1037 (1957).

[5] Cork, Lambertson, Piccioni, and Wenzel, Phys. Rev. **104**, 1193 (1956).

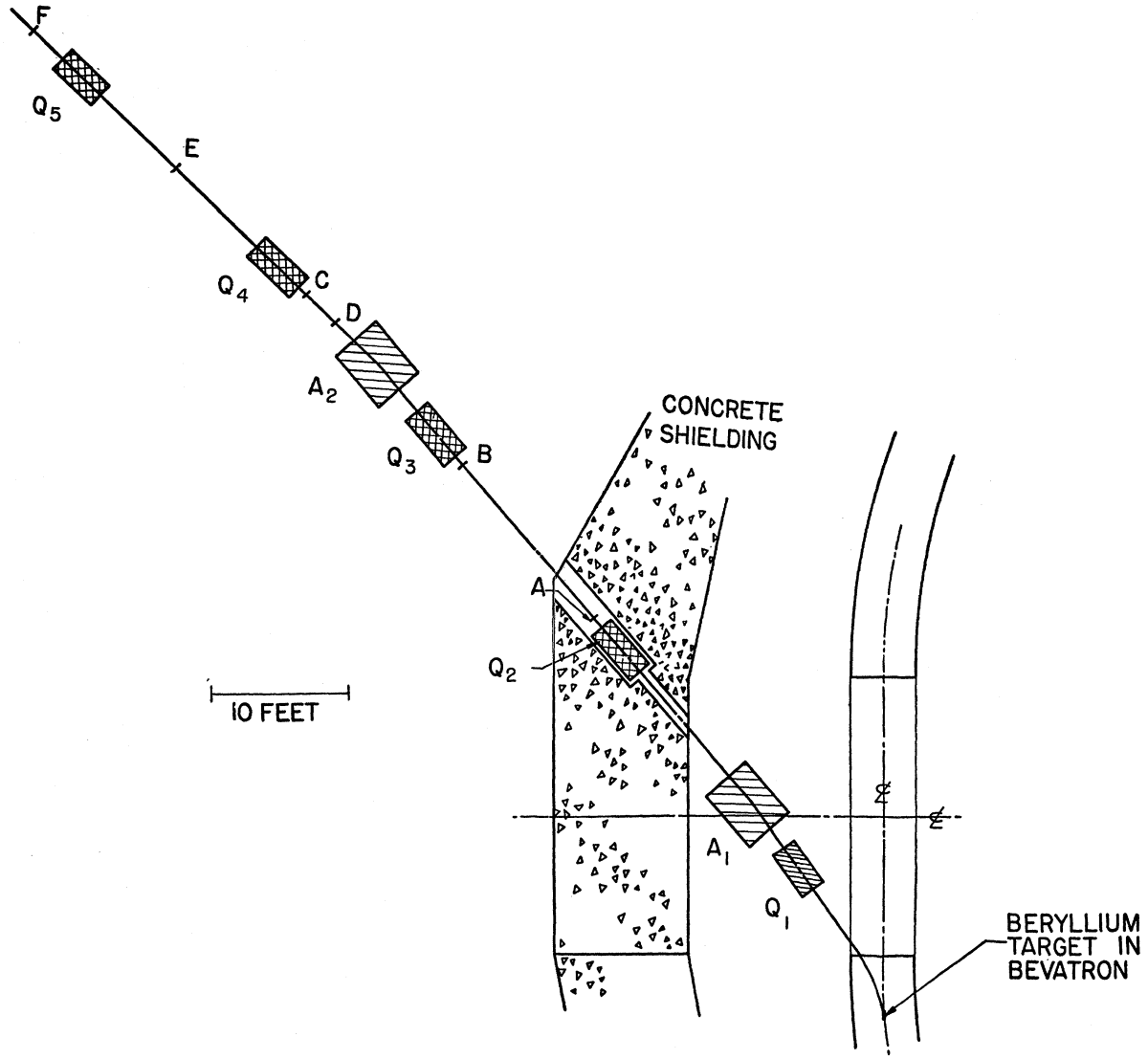

FIG. 1. Antiproton selecting system. Q_1 through Q_5 are three-element quadrupole lenses and A_1 and A_2 are beam-deflecting magnets. A through F are plastic scintillation counters.

From this point at 5° from the end of the quadrant, negative particles produced in the forward direction were deflected by the magnetic field toward a thin ($\frac{3}{16}$-inch) section of the vacuum-tank wall.

The external beam channel (Fig. 1) was designed to carry a beam of considerable momentum width over the required time-of-flight path. Five quadrupole lenses of nominally 4-inch aperture were employed; each lens was composed of two quadrupoles 8 inches long and one 16 inches long. The first lens, Q_1, was placed as close as feasible (130 inches) to the internal target so as to obtain the maximum solid angle of acceptance. To attain sufficient focusing power from available units and to allow some choice in magnification, the three quadrupoles in Q_1 were arranged to function as a two-element lens. The two 8-inch units were adjacent with their fields aiding and in a direction opposite to that in the 16-inch quadrupole that followed; a 7.25-inch interval between these quadrupoles was the minimum allowed by the water and electrical connections. Q_1 formed an image of the beryllium target at the entrance to Q_2 and effected a transition into the repeating pattern of lenses that followed. Each of the four lenses after Q_1 was adjusted to focus particles emerging from the lens preceeding it into the aperture of the succeeding lens. For particles at the center of the momentum interval accepted, lenses Q_2 and Q_4 were located at the target image points, and in this sense bear some analogy to field lenses in an optical system. Such an array of lenses uniformly spaced at twice the focal length presents a good aperture to particles from an extended source and over a broad

momentum range; it is a feature of this system that the aperture remains large when the channel is lengthened by the addition of lenses. The broad admittance of this beam channel not only permitted a large flux of particles, but also reduced beam loss from scattering in the vacuum-tank wall and in the scintillators. Our lenses Q_2 through Q_5 were each symmetric arrangements of quadrupoles with the 16-inch unit in the center separated from the 8-inch units by 10.5-inch intervals. The series of magnetic lenses carried negative particles a distance of about 100 feet from the target. At 1.4 Bev/c momentum, the lenses after Q_1 operated with gradients of about 3600 gauss/inch; Q_1 had about 2800 gauss/inch, and the lenses were spaced with 251 inches between centers.

The dispersion of the magnetic field in the Bevatron produced a horizontal extension of the target image at Q_2. The magnification of Q_1 and deflection in the first analyzer magnet, A_1, increased this effect and allowed adjustment of the momentum interval entering the aperture of Q_2. The analyzer magnets also served to reject positive particles that scattered into or were produced along the beam path.

Principal considerations affecting a choice of momentum interval were the maximum permissible counting rate in the first scintillator (A in Fig. 1), and the spread in time of flight of antiprotons over the 65-foot timing path used to distinguish antiprotons from lighter particles. A momentum interval of $\pm 5\%$ was chosen at each momentum used.

To change the average momentum of the particles carried by the channel, it was necessary to swing the entire set of magnets about to a new direction. The highest value of momentum reached in this experiment was determined by the requirement that the antiprotons have a velocity detectably different from that of π mesons. Toward lower momenta, the flux of antiprotons became small. Limiting values of momenta used were 0.75 Bev/c and 1.42 Bev/c.

The magnetic system transmitted a beam of about 5×10^4 particles per 10^{10} primary protons. At 18 feet beyond the final quadrupole, the beam was half-maximum intensity on a circle of about 3 inches diameter.

III. ELECTRONICS

Figure 2 shows a block diagram of the basic electronics. Antiprotons were selected by the coincidence of pulses from six scintillation counters spaced as shown in Fig. 1. These were combined in two fast triple-coincidence circuits, C_1 and C_2, each with a resolution of the order of 2×10^{-9} second (Fig. 2), followed by another coincidence circuit of resolution 2×10^{-8} second, which included as well the pulse from the final counter, L. The coincidence output from each of these circuits was fed to a fast discriminator and pulse shaper followed by another set of coincidence circuits of 10^{-7} sec resolving time. The output of each of these was shaped and fed to the scalers. Simultaneously, an oscilloscope was triggered, and pulses from Counters A, F, and L were displayed to furnish a check on the accidental rate and to indicate in another way the transmission of the hydrogen target for antiprotons. The vertical position of the oscilloscope trace was displaced a few millimeters after each trace. In this way a number of antiprotons could be recorded during each Bevatron pulse. The oscilloscope face was photographed on 35-mm film moving at a steady rate of 0.8 in./min.

Each of the plastic scintillators, A through F, was 0.25 in. thick and about 4 by 4 inches in area to cover the aperture of the magnetic system. These were viewed through Lucite light pipes by RCA-6810 fourteen-stage photomultipliers which fed directly into the fast-coincidence circuits.

In addition, three monitors were provided. A scintillation telescope M_1, looking directly at the internal target, monitored the beam spill-out. A coincidence circuit M_2, connected to alternate outputs of Counters C and E and timed to count π mesons, monitored the channel flux; and the signal from a beam induction electrode in the Bevatron was integrated to provide a record of the total circulating beam.

The structure of the Bevatron circulating beam during acceleration has pronounced rf modulation. To reduce the peak counting rate encountered by our time-of-flight scintillators, the following beam spill-out technique was employed. The circulating proton beam was steered into a thin aluminum foil (0.0003 inch) at the outer radius. The energy loss sustained in repeated passage through this foil caused the protons to become phase-unstable and to spiral inward in the increasing magnetic field of the Bevatron. In the several milliseconds required to spiral into the beryllium target all phase coherence was lost, and a beam spill-out of uniform intensity was obtained. By control of the rate at which the initial beam was driven into the foil,

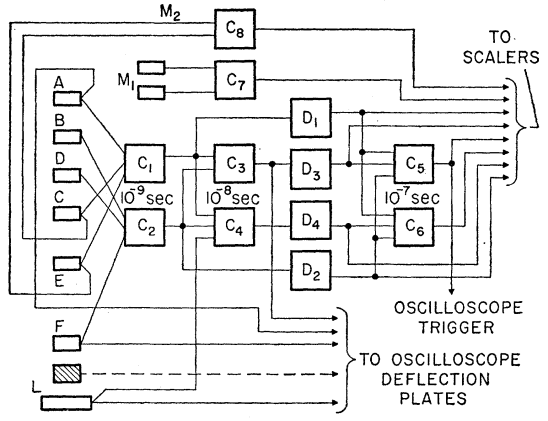

FIG. 2. Block diagram of basic electronics. A through L are scintillation counters; C_1 through C_8 are coincidence circuits; D_1 through D_4 are discriminators. M_1 and M_2 are monitors of the internal target and the magnetic channel flux, respectively. Amplifiers are not shown.

the length of the spill-out could be adjusted. In this experiment, a 100-millisecond spill was used, corresponding to an energy range of the internal beam of from 5.8 to 6.2 Bev.

IV. IDENTIFICATION OF ANTIPROTONS

The intervals AC, CE, BD, and DF between counters were each long enough to reject single π mesons by a large factor ($\approx 10^3$) when the counters were timed for antiprotons ($\beta \approx 0.625$ to 0.83). Similarly, twofold accidentals were rejected because, for example, two mesons that simulated an antiproton in the interval AC could not simultaneously do so in the interval CE. The use of two such coincidence circuits serves a double purpose. First, the probability that an accidental coincidence occurs in two slightly detuned independent circuits is the product of the probabilities for each. Thus the rejection of mesons is improved. In addition, some rejection against threefold accidentals can be obtained by staggering the intervals so that we have $AC > CE$ while $BD < DF$. Separation of the antiprotons was, of course, most difficult at the highest velocity employed ($\beta = 0.83$). The lengths of the cables connecting each counter with the coincidence circuit determined the velocity to which the electronic system was sensitive, and therefore defined the mass of particles selected. Figure 3 shows the number of coincidences obtained at 1.4 Bev/c as the relative counter delays were adjusted to detect particles of different masses. The positions of π^- mesons, K^- mesons, and antiprotons on this scale are indicated. Separation of the antiprotons is shown to be very complete. In fact, there is evidence to indicate that for a cable delay of about two feet from the π meson peak, the delay curve is widened by the presence of K^--meson contamination of the beam. An accidental coincidence appeared on the oscilloscope trace as a double pulse in the A counter; this type of event accounted for no more than a few percent of all traces.

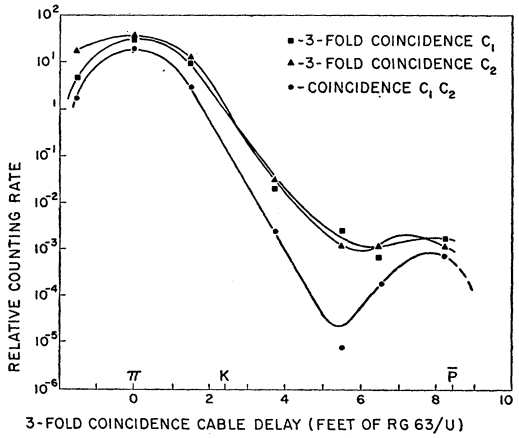

FIG. 3. Delay curve of time-of-flight selector at 1.4 Bev/c. Calculated delays for π^- mesons, K^- mesons, and antiprotons are shown on the horizontal axis. Coincidence C_1C_2 is made between the outputs of the two threefold coincidence circuits.

TABLE I. Observed yields of antiprotons and π^- mesons in a momentum interval of $\pm 5\%$.

Average momentum ($\pm 3\%$) (Bev/c)	Angle of emergence at target (degrees)	Solid angle (10^{-3} sterad)	$\bar{p}/\pi^-$ ($\pm 60\%$)	π^-/proton ($\pm 60\%$)	$\bar{p}$/proton Observed ($\pm 30\%$)	$\bar{p}$/proton Predicted yield[a] (relative to yield at 0.75 Bev/c)
0.75	8.5	0.61	2×10^{-6}	0.8×10^{-6}	1.5×10^{-12}	1.0
0.90	3.0	0.57	4×10^{-6}	1.2×10^{-6}	4.6×10^{-12}	3.5
1.15	2.5	0.54	12×10^{-6}	2×10^{-6}	20×10^{-12}	7
1.41	6.2	0.52	19×10^{-6}	2.5×10^{-6}	58×10^{-12}	12

[a] See reference 7.

As an additional reality check at 1.15 Bev/c, a Čerenkov counter containing Fluorochemical 0–75[6] (index of refraction = 1.27) was temporarily placed behind F and put in anticoincidence in C_3 (Fig. 2). This gave very high rejection of π mesons with relatively low rejection of the antiprotons.

The yields of antiprotons and of π^- mesons are given in Table I. The numbers are those actually observed with no correction for inefficiency, attenuation, and scattering in our detecting system. A distortion of the production spectrum also results from the thickness of our beryllium target. Thus, it is possible to say only that there is fair agreement with the relative numbers for antiproton production as obtained from phase-space calculations[7] listed in the last column of Table I.

V. HYDROGEN TARGET AND ATTENUATION EXPERIMENT

The absorber thickness chosen for an attenuation experiment depends on a number of factors, but when the limitation on accuracy is expected to be set largely by counting statistics, a thickness on the order of one mean free path is desirable. Previous measurements of the interaction of antiprotons in matter had indicated that the total cross section is quite large,[1–4] and would probably be large in pure hydrogen. However, the thickness of hydrogen needed to assure efficient use of the antiprotons was still rather great. Accordingly, a liquid hydrogen target 62 inches long (11.3 grams) was constructed for this experiment (Fig. 4). Since the diameter of the beam was defined by the quadrupole focusing magnets and the 4-by-4-inch counters, a target of 8-inch diameter was sufficient. The target has a volume of 50 liters and the reservoir approximately 2 liters. This volume is sufficiently great so that safety precautions as well as good insulation were important considerations. The liquid hydrogen cylinder was supported in a vacuum (less than 10^{-5} mm Hg) by radial cables, and surrounded by heat shields inside a liquid nitrogen jacket. The liquid nitrogen was insulated by Styrofoam and Santocel.

[6] Minnesota Mining and Manufacturing Company.

[7] Chamberlain, Chupp, Goldhaber, Segrè, Wiegand, Amaldi, Baroni, Castagnoli, Franzinetti, and Manfredini, Nuovo cimento **3**, 447 (1956).

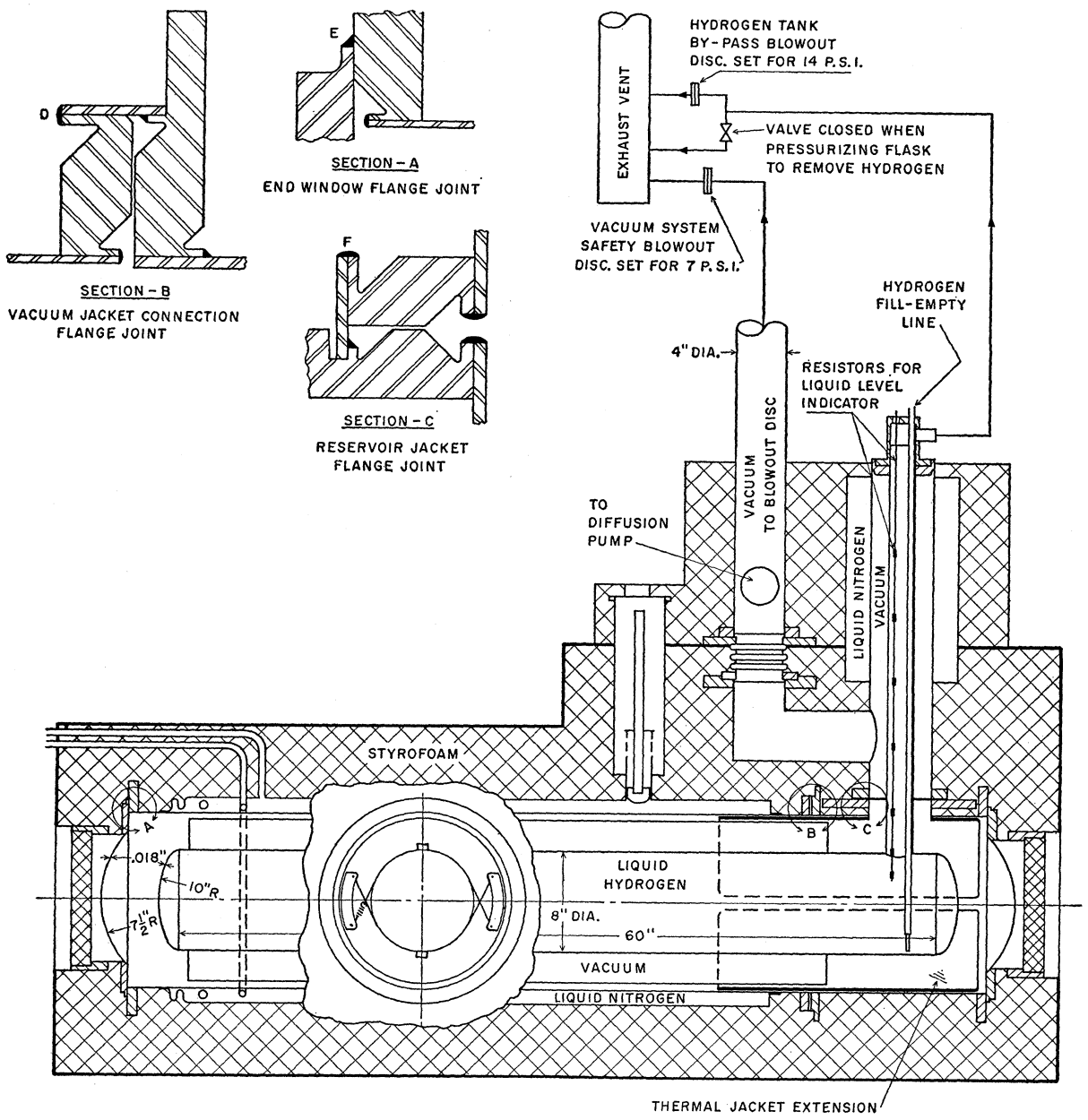

FIG. 4. Diagram of liquid hydrogen target construction.

The target was made of 310 stainless steel, heliarc-welded. (See UCRL Engineering Note 7307-01-M16.) The target can be disassembled by grinding the cylindrical welds. Each of the end windows is of spun stainless steel 0.020 inch thick. The four steel windows through which the beam passed totaled about 2 g/cm^2. The hydrogen container was tested at a hydrostatic pressure of 130 lb per in.^{2} During operation the target was vented to the roof of the building. The target used approximately 1.5 liters of liquid hydrogen per hour provided the reservoir was only partially filled. The hydrogen could be put in or removed in about 15 minutes. At each energy several runs with and without hydrogen were made.

The geometry for L (Fig. 5) was chosen so that the half-angle subtended by L at the target was as small as possible consistent with negligibility of uncertainty due to multiple Coulomb scattering and the natural spread of the beam from the selecting system. In this way the uncertainties due to forward scattering and annihilation secondaries were minimized.

Figure 6 shows the experimental results obtained at each energy. Values for the transmission of the hydrogen target, as obtained from the scalers and from the

oscilloscope, are in good agreement. Cross sections in the figure are those obtained from the oscilloscope, which was less sensitive than the scaler readings to fluctuations in the pulse height from L. Uncertainties indicated are statistical only.

Determination of the total cross section for the interaction of antiprotons with protons requires a correction for the finite solid angle subtended by Counter L at the target. The value of this correction may be estimated from the formula relating the imaginary part of the forward scattering amplitude, I_0, to the total cross section σ_T.[8]

$$I_0=\sigma_T/(4\pi\lambda\!\!\!^{-}),$$

where $\lambda\!\!\!^{-}$ is the wavelength of the incident antiproton. The magnitude of the correction for forward scattering is given by

$$\Delta\sigma=(d\sigma/d\Omega)_0\Delta\Omega_0=(I_0^2+R_0^2)\Delta\Omega_0,$$

where $\Delta\Omega_0$ is the average solid angle subtended by L at the hydrogen target, and R_0 is the real part of the forward scattering amplitude. Hence

$$\Delta\sigma=(\sigma_T/4\pi\lambda\!\!\!^{-})^2\Delta\Omega_0 \qquad (1)$$

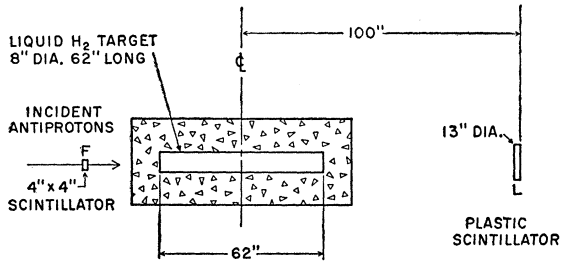

FIG. 5. Layout of attenuation experiment with hydrogen target.

gives a lower limit to the correction to the cross section. If the $\bar{p}$-p interaction is largely inelastic—a plausible assumption in view of previous results obtained with heavy matter[1-3]—then R_0 is small compared with I_0, and the value for $\Delta\sigma$ given by (1) represents with sufficient accuracy the required correction. This correction, which amounts to about 2 mb at each energy, has been added to obtain the corrected cross sections given in Fig. 6.

Charged annihilation secondaries passing through L would reduce the apparent cross section. From the geometry used in each case, this effect has been calculated on the assumption that each interaction produces, on the average, n fast charged secondaries emitted isotropically in the center-of-mass system. Emulsion experiments indicate that $n\approx 3.5$.[4] From this value it is estimated that at each energy the measured cross sections are about 1% to 2% low. This estimate is not very sensitive to the assumed energy distribution of the secondaries in the center-of-mass system.

[8] H. A. Bethe and F. de Hoffman, *Mesons and Fields* (Row, Peterson and Company, New York, 1950), Vol. II, p. 76.

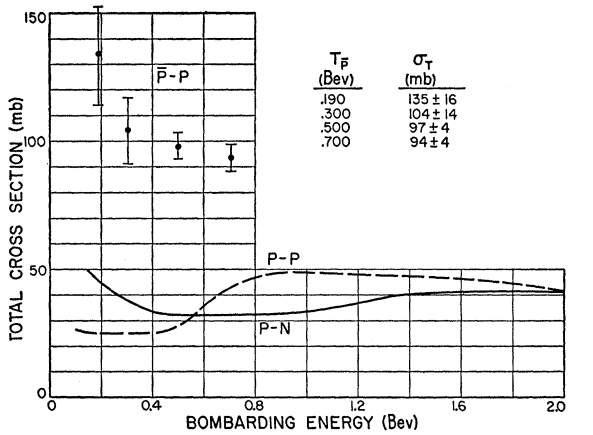

FIG. 6. Total antiproton-proton cross-section results. Uncertainties given are statistical only. Cross sections for p-p and p-n interactions are shown for comparison.

Contamination of the beam of antiprotons may involve accidental coincidences of more than one π meson. Continual checks on the oscilloscope traces indicated that this is certainly less than 5% and probably no more than 2%. By the use of the information on the oscilloscope, accidental coincidences could, of course, be rejected. At 1.4 Bev/c the accidentals could not be separated with certainty, and on the basis of the delay curve (Fig. 3) we assumed an upper limit of about 3% for the contamination. No correction for this effect or for the effect of annihilation secondaries has been made to the values in Fig. 6.

VI. ANTIPROTON CROSS SECTIONS IN BERYLLIUM, CARBON, AND LEAD

A. Beryllium

The same method as was used in the hydrogen cross-section measurements was used to measure the total cross sections of antiprotons in beryllium for bombarding momenta of 1.4 and 1.15 Bev/c. Results are shown in Table II. The half-angles used were again large enough to include the multiple Coulomb scattering. In this case, however, the correction for forward nuclear scattering is much larger. The correction has been made with the assumption that the forward scattering is a diffraction effect resulting from absorption over a uniform partially transparent disk of radius 3×10^{-13} cm, but the amount of this correction is found be insensitive to the disk radius assumed. Uncorrected and corrected values for the cross section are given.

TABLE II. Cross sections for antiprotons on beryllium.

Target thickness (g/cm²)	$T_{\bar{p}}$ (Mev)	$\theta_{\frac{1}{2}}$ (degrees)	Total cross section σ_{obs} (mb)	σ_{cor} (mb)
27.9	500	2.57	460	484±60
24.4	700	3.65	367	415±65
24.4	700	1.90	416	435±75 } Av 425±50

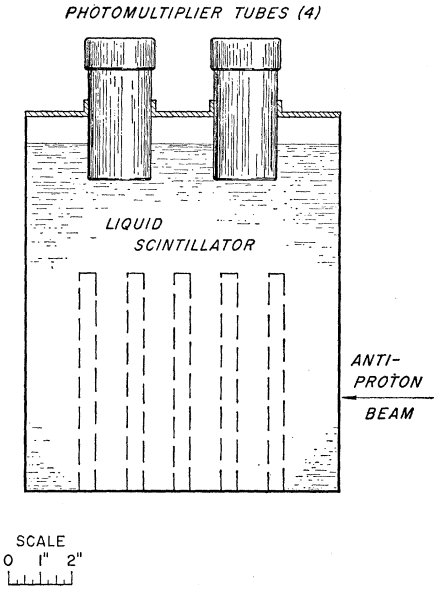

FIG. 7. Liquid scintillator target assembly. The dashed outlines indicate the location, when in place, of wafer inserts of target material.

The uncertainty expressed is statistical only. The energies given in the table correspond to the antiproton kinetic energies at the center of the Be target and are uncertain by $\pm 5\%$.

B. Carbon

In order to measure the cross section for antiprotons on carbon a somewhat different method was tried. This centered around the use of the "live" target, X, consisting of a 5-gallon liquid scintillator located behind Counter F (see Fig. 7). Each time an antiproton was selected by the time-of-flight system, the pulse produced by this large scintillator was photographed. By pulse-height analysis, antiprotons that interacted inelastically could be separated from those that either scattered elastically or passed through without interaction.[5] Simultaneously the 13-inch final counter L was located beyond the target in order to detect transmitted antiprotons. The spectrum of pulse heights in X for 330 incident antiprotons of momentum 1.4 Bev/c with L in "good" geometry ($\theta_{\frac{1}{2}}=2.65°$) is shown in Fig. 8. Pulses are separated into two groups according to whether or not a coincident pulse occurred in L. The sharply peaked upper spectrum of Fig. 8 indicates that L detects principally noninteracting and forward-scattered antiprotons. A small number of secondaries associated with inelastic events in X (larger pulses) are detected by L. On the other hand, events that are not detected in L are principally inelastic, as is indicated by the broad lower spectrum of Fig. 8. The peak in this spectrum is attributed to antiprotons that scatter elastically at angles large enough to miss counter L.

Figure 9 shows a similar spectrum obtained for 1959 antiprotons incident upon X with L placed in "poor" geometry ($\theta_{\frac{1}{2}}=25°$). The broad background of the upper spectrum of Fig. 9 indicates that relatively more secondaries are detected by L, and the absence of a peak in the lower spectrum indicates that elastically scattered antiprotons are contained within L.

From the spectra of Fig. 8 we have determined the total carbon-antiproton cross section. Results of the cross-section measurements for hydrogen described in Sec. V have been used to correct the observed transmission of toluene (C_7H_8) to obtain the transmission for pure carbon.

From the spectra of Fig. 9 we have determined the inelastic carbon-antiproton cross section. Correction for hydrogen absorption has been made with the assumption that the proton-antiproton cross section is three-fourths inelastic. The justification for this is that, as will be seen, the inelastic antiproton cross section for

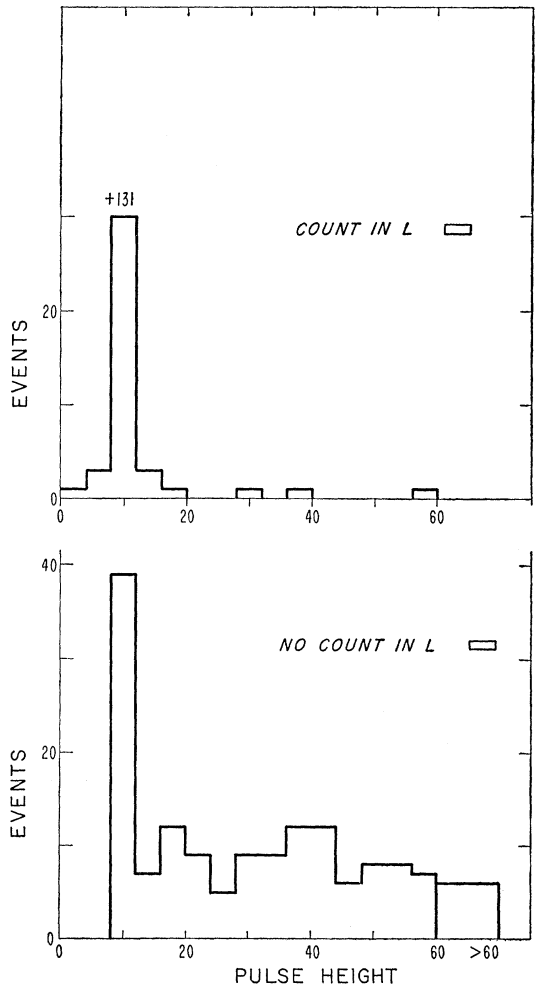

FIG. 8. Pulse-height spectra in X for incident 1.4-Bev/c antiprotons. The 330 events are separated according to whether or not a coincident count occurred in a scintillator, L, which subtended at X an angular half-width of 2.65°.

carbon, and probably for beryllium, is considerably larger than the elastic. Since the total correction for hydrogen absorption amounts to only 15% of the carbon-antiproton cross section, the uncertainty introduced by this assumption is small.

The forward-scattering correction to the total cross-section measurement has been made, as for the beryllium measurements, by assuming that the region of interaction is an absorptive disk. The correction, although rather large, is relatively independent of the assumed radius of interaction. The value for the corrected total cross section $(\sigma_T)_{cor}$, given in Table III, is obtained for that radius which gives a computed value for the inelastic cross section equal to the measured value. The table includes as well the results of similar measurements at 0.9 Bev/c. $T_{\bar{p}}$ is the kinetic energy of the antiproton at the center of the carbon (toluene) target and is uncertain by $\pm 5\%$. The expressed uncertainties in the cross sections are statistical only.

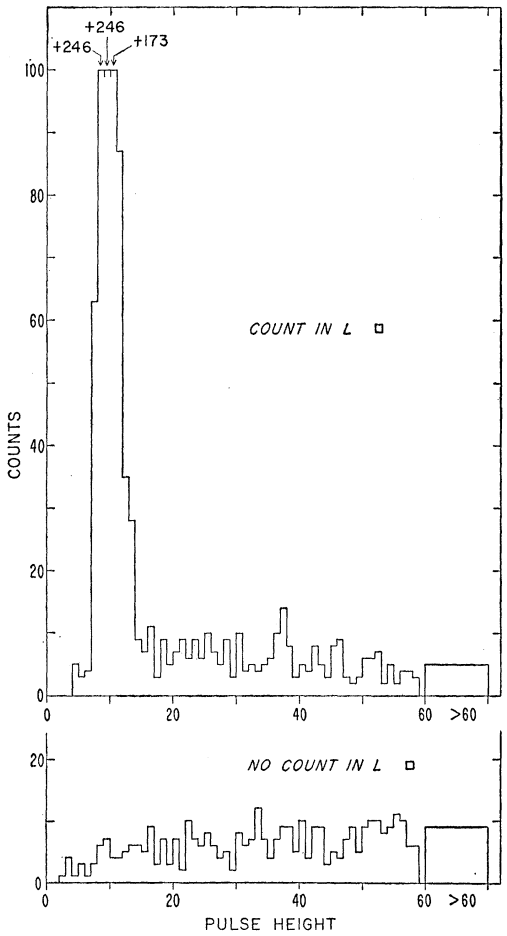

FIG. 9. Pulse-height spectra in X for incident 1.4-Bev/c antiprotons. These 1959 events are also separated as in Fig. 8, but with L subtending a half-angle of 25° in this case.

TABLE III. Cross sections for antiprotons on carbon.

$T_{\bar{p}}$ (Mev)	$\theta_{\frac{1}{2}}$ (degrees)	σ_{in} (mb)	$(\sigma_T)_{obs}$ (mb)	$(\sigma_T)_{cor}$ (mb)
700	25	436±19		
700	2.64		575±59	657±79
300	3.55	568±102		
300	3.55		618±111	655±130

C. Lead

The desirability of extending the measurement of antiproton cross sections to elements other than carbon suggested the use of wafer inserts in the toluene scintillator. This might be especially helpful for heavy elements, for which the performance of good-geometry attenuation experiments is complicated by the large multiple Coulomb scattering produced by thick targets. To try this method, five equally spaced half-inch lead wafers were placed in X (dashed outlines in Fig. 7).

From the transmission of X for antiprotons with and without lead inserts, the inelastic antiproton-lead cross section has been computed to be 2330 mb±285 mb at 650 Mev. The expressed uncertainty is statistical only. Other uncertainties in the lead-wafer experiment are probably greater than in the carbon experiment. The presence of the wafers reduces the light-collection efficiency and the uniformity of the scintillator; some self-absorption of inelastic events occurs in the wafers; and finally the larger Coulomb scattering associated with the lead target makes the final counter L less helpful in separating elastic and inelastic events.

CONCLUSIONS

The total proton-antiproton cross section is about 100 mb in the energy range of 300 to 700 Mev. This is considerably larger than the nucleon-nucleon cross sections for the same range of bombarding energies (see Fig. 6), and is apparently a direct consequence of the annihilation interaction. This interpretation is supported by measurements with a "live" target which show that in carbon the inelastic cross section is about twice the elastic cross section. Annihilation processes are a large part of these inelastic events, as indicated by the pulse-height spectrum (see Fig. 9). It is not surprising that we find relatively fewer inelastic interactions involving meson production without annihilation. These interactions are expected to occur through processes similar to those operating in the nucleon-nucleon and pion-nucleon interactions, for which the high-energy inelastic cross sections are about 30 mb. Direct observation has shown that the charge-exchange cross section for antiprotons on CH is of the order of a few millibarns.[5]

Comparison of our value of 484±60 mb for the total antiproton-beryllium cross section at 500 Mev and the previous value of 365±59 mb for the cross section obtained in a "poor" geometry experiment[2] indicates

that for beryllium also the inelastic antiproton cross section is probably considerably larger than the elastic.

Part of the difference between the nucleon-nucleon and nucleon-antinucleon cross section may follow from the large energy available (approximately 2 Bev) in the annihilation process. This factor, however, is not by itself sufficient to account for the large difference when we recall that for the p-p interaction at 5.3-Bev bombarding energy, where the center-of-mass energy is about the same as that of the nucleon-antinucleon system being considered, the total cross section is actually somewhat less[9,10] than that at 0.8-Bev bombarding energy.[11] Therefore, the large magnitude of the nucleon-antinucleon cross section, as compared with the nucleon-nucleon cross section, seems to be a characteristic of the basic nucleon-antinucleon interaction. An interesting approach in arriving at a theoretical formulation for such an interaction has been followed by Duerr and Teller.[12,13]

In the description of high-energy nucleon-nucleon and pion-nucleon collisions it is often convenient to speak of a radius of interaction. This is meaningful if the wavelength of the interacting particles is somewhat less than the radius R obtained, for example, by setting $\pi R^2 \approx \sigma_T$, where σ_T is the measured total cross section. Proceeding similarly, we see that the antiproton-proton interaction is characterized by a "radius" about equal to the spacing between nucleons in the nucleus, so that we expect the nucleus to be relatively opaque to antiprotons. The extent of the interaction outside the nucleus is determined by interaction with nucleons on the surface. Consequently, in interactions with nuclei the ratio between the cross section for antinucleons and that for nucleons is expected to be smaller for the heavier nuclei. This is consistent with our observation that the inelastic antiproton-lead cross section is only 1 to 1.5 times the proton-lead cross section measured by Chen, Leavitt, and Shipiro,[14] while for the lighter elements the factor is about 2.

The yield of antiprotons produced from 6-Bev protons incident upon a beryllium target is a strong function of antiproton energy, and is in fair agreement with the phase-space calculations.[7]

Uncertainties given in each case are statistical only. Certain systematic uncertainties have been discussed separately in connection with the particular results.

ACKNOWLEDGMENTS

We take this opportunity to thank Dr. Edward J. Lofgren and the Bevatron operating staff for their invaluable cooperation. The help of Laurence S. Beller, Charles A. Coombes, Fred H. G. Lothrop, and Douglas Parmentier during the experiment is greatly appreciated. The liquid hydrogen target was designed by William M. Salsig and Garth E. Cook. Marion J. Jones was responsible for the design and operation of the numerous magnet power supplies. A group working with Felix C. Caldera built much of the electronics.

[9] Wright, Powell, Maenchen, and Fowler, Bull. Am. Phys. Soc. Ser. II, **1**, 376 (1956).
[10] Cork, Wenzel, and Causey, Bull. Am. Phys. Soc. Ser. II, **1**, 376 (1956).
[11] Chen, Leavitt, and Shapiro, Phys. Rev. **103**, 211 (1956).
[12] H. Duerr and E. Teller, Phys. Rev. **101**, 494 (1956).
[13] H. Duerr, Phys. Rev. **103**, 469 (1956).
[14] Chen, Leavitt, and Shapiro, Phys. Rev. **99**, 857 (1955).